IEEE Access
Multidisciplinary | Rapid Review | Open Access Journal

Received 14 November 2023, accepted 5 December 2023, date of publication 18 December 2023,
date of current version 22 December 2023.

Digital Object Identifier 10.1109/ACCESS.2023.3344155

RESEARCH ARTICLE

Active Heat Flow Sensing for Robust Material Identification

YUKIKO OSAWA, (Member, IEEE), KEI KASE, (Member, IEEE), YOSHIYUKI FURUKAWA, AND YUKIYASU DOMAE, (Member, IEEE)
Industrial Cyber-Physical Systems Research Center, National Institute of Advanced Industrial Science and Technology (AIST), Tokyo 135-0064, Japan
Corresponding author: Yukiko Osawa (yukiko.osawa-akiyama@aist.go.jp)

This work was supported by the Japan Society for the Promotion of Science (JSPS) KAKENHI under Grant 23K13303.

ABSTRACT Thermal properties are significant for recognizing an object's material but cannot be determined via visual and stiffness (or tactile) –based recognition techniques. Most studies have used temperature as a complementary part of multimodal sensing; however, the thermal signal is an unexplored capability that can be beneficial for recognizing target objects. Since changes in thermal responses can result from both material properties and initial temperature, realizing robust and high-accuracy recognition in different environments is a challenging issue. To tackle the issue, this paper proposes a novel strategy for material identification that can actively measure heat flow by heating and cooling a robot gripper, enabling the extraction of the thermal properties of contact materials regardless of the object's initial temperature variation (referred to as ''active heat flow sensing''). We use a robotic task as an example of one possible application of the proposed strategy. For this, we developed a gripper pad embedded in a temperature control system and heat flow sensor to monitor the thermal exchange during contact with a target object. The paper conducted some experiments divided into two scenarios. The first experimental results show that active heat flow sensing is realized within 0.4 sec from first contact for 100 % classification of four heated materials. The second experimental results show that the three materials, whose thermal properties are largely different, can be classified within 0.7 sec from first contact using different initial temperatures of the training and test data. These results suggest robustness against environmental change, which has been difficult using conventional temperature-based methods.

INDEX TERMS Heat flow, material properties, temperature control, thermal sensing.

I. INTRODUCTION

Object recognition can enhance a robot's perception, allowing it to take the object's shape, surface, and certain properties into account for robotic motion planning. Material recognition is a key technique used to recognize target objects by extracting material features such as roughness, compliance, slipperiness, and coldness [1]. Previous works in material recognition have used contact sensing (e.g., tactile sensor), contactless sensing (e.g., proximity sensor), or both.

Vision sensors [2], [3], capacitive sensors [4], [5], or proximity sensors [6] such as radar [7], ultrasound and lasers [8], [9] are generally used for contactless sensing. Contact sensing by tactile sensors can directly measure surface texture and stiffness [10], [11] without high computational cost. Various robot motions allow tactile sensors to capture unique characteristics of the target object: e.g., roughness and friction coefficient by sweep motion [12], stiffness by grasping motion [13], hardness by pressing [14], sounds by knocking and grasping [15], and fabric properties by squeezing [16]. An approach that combines tactile and vision sensors can compensate for the drawbacks of contact sensing: low sensor resolution and low durability. In [17], a tactile sensor with

The associate editor coordinating the review of this manuscript and approving it for publication was Lei Wei.

depth and RGB images was employed to recognize objects. Furthermore, in [18], tactile and vision sensors were utilized in the learning process, with only the vision data used during the recognition phase to avoid sensor deterioration. Moreover, multimodal sensors, including pressure, vibration, temperature, etc., have also been developed [19], [20], [21], [22], [23], [24] to improve the sensing performance.

Among them, thermal sensing is essential to extract an object's thermal properties [25], [26], [27]; it is useful to recognize objects with similar stiffness and roughness values, often being included as one of the elements of the multimodal sensors. As the heat flow sensor tends to have a hard surface and the cost is expensive, a temperature sensor, which is a tinier and cheaper sensor, is mainly used for robotic applications. Thermal-based recognition methods have been studied for many years [28], [29], [30], [31], and knowledge has been utilized to stimulate human thermal perception [32], [33], [34], [35]. Moreover, the classification accuracy and the response speed have been improved using machine learning [36], [37]. The study [38] has developed a specific sensing system for material classification using multiple temperature sensors to measure the heat flow.

Most studies assume that the targeting objects are at room temperature and are recognized under the same environment as the case of learning data acquisition. However, both temperature and heat flow responses change depending on initial temperature variations of the robot's surface and the target object, which affects the classification accuracy [39]. In particular, the material properties cannot be revealed when the initial temperature of a robot and an object is the same. Therefore, high-accuracy recognition independent of the initial temperature is a challenging issue, and thermal-based recognition is sensitive to environmental changes and is mainly used as a subsidiary and complementary element of multimodal sensing. These studies [24], [40] tackled the issue; however, more investigation in terms of various initial temperatures in the training and test phases is needed to improve the thermal-based method. The authors believe that improvements in thermal sensing significantly advance multimodal sensing techniques.

II. CONTRIBUTION AND OVERVIEW

In this paper, instead of temperature data, heat flow data is used for material identification to handle initial temperature variations, which directly expresses the amount of thermal exchange. The proposed recognition system includes a temperature control system. Thus, the temperature of a contact surface can be actively controlled to generate a temperature difference with the contact object to induce heat flow in any case (referred to as "active heat flow sensing" in this paper).

The strategy is implemented by using the grasping motion of a robot gripper as an application of a robotic task (see Fig. 1). Experiments at various initial temperatures were conducted using the developed gripper pad attached to the gripper, showing robust material identification using active heat flow sensing. There has yet to be a robot gripper capable of active thermal control with heat flow sensing for material identification.

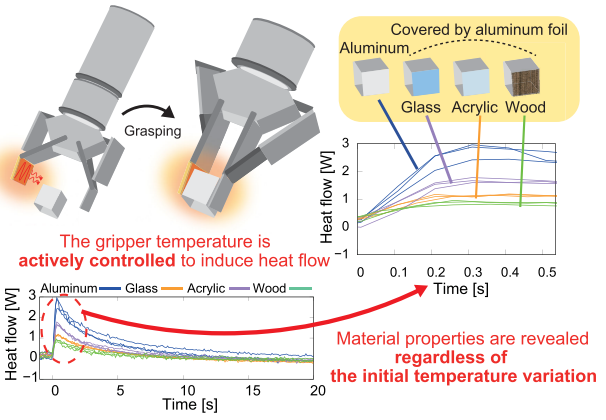

FIGURE 1. The proposed active heat flow sensing scheme. The proposed system can induce and monitor heat flow between a gripper and various material objects by actively controlling the robot gripper's surface temperature and extracting the objects' material properties for identification.

As the paper's contribution is a novel system design to derive thermal data correction, any neural network method is acceptable for material classification in our system. Besides, recurrent neural networks (RNNs) can learn features and long-term dependencies from sequential and time-series data with its context layers and can learn various dynamical systems. A long short-term memory (LSTM) neural network is one of the most used types of RNN model that can consider both the system's short- and long-term dynamics. Thus, we used LSTM for material classification in this paper. We also used primary RNN for comparison.

The proposed active heat flow sensing scheme consists of a gripper pad to monitor the thermal exchange with the object in contact and a temperature control system using circulating water. The thermal contact model is explained in Sec. III, and Sec. IV presents the active heat flow sensing apparatus, including the gripper pad design and the water system. This paper used an aluminum cube and three kinds of solid materials wrapped in aluminum foil as contact objects, making it difficult to distinguish visual and tactile sensing. The obtained heat flow responses are used as inputs of the LSTM neural network, showing the validity of the active heat flow sensing concept. The experimental results are shown in Sec. V. The paper is concluded in Sec. VI and Sec. VII.

III. THERMAL CONTACT MODEL

A. HEAT FLOW AND TEMPERATURE

In this section, "heat flow," which is used as an input for material identification, is explained. In this study, the thermal model of a contact surface between a gripper and an object is simplified as one-dimensional heat transfer as

$$\frac{\partial T}{\partial t} = \alpha \frac{\partial^2 T}{\partial x^2}, \tag{1}$$

where T, t, x, and α stand for temperature [K], time [sec], heat transfer direction [m], and heat diffusivity [m^2/s], respectively. Equation (1) in the steady state ($t = \infty$) without heat generation is presented as

$$\alpha \frac{\partial^2 T}{\partial x^2} = 0 \tag{2}$$

When two materials (gripper and contact object in this paper) physically contact each other (the boundary condition: T_g at $x = 0$, and T_o at $x = L$, see Fig. 2A), the temperature variable is derived from (2) as

$$T(x) = T_g - \frac{x}{L}\left(T_g - T_o\right), \tag{3}$$

where T_g, T_o, and L denote the temperature [K] of the gripper, the temperature [K] of the object, and the heat transfer distance [m] (thickness of the heat flux sensor), respectively.

In addition, the heat transfer rate (called "heat flow q [W]") is shown as

$$q = -\lambda A \frac{\partial T}{\partial x}, \tag{4}$$

where λ and A denote the heat conductivity [W/mK] and cross sectional area [m^2], respectively. Here, the heat flow rate per unit area and per unit of time (see Fig. 2B) is called the "heat flux φ [W/m^2]" as

$$\varphi = -\lambda \frac{\partial T}{\partial x} \tag{5}$$

Using (3), the heat flow in (4) can be described as

$$q = \frac{T_g - T_o}{L/\lambda A} = \frac{T_g - T_o}{R_{con}}, \tag{6}$$

where R_{con} is defined as the thermal contact resistance (*TCR*) in [K/W]. This assumes that the thermal transfer is related to the electric circuit (called the thermal network method, see Fig. 2C). Based on the electrical system's analogy, heat flow is equivalent to the flow variable as current, whereas temperature is the effort variable as voltage. Equation (6) can be interpreted as Ohm's law; that is, the flow variable is proportional to the difference in the effort variable. Therefore, heat flow can directly express the amount of thermal exchange between the gripper and the object. This is an appropriate variable for material identification that can describe thermal evolution regardless of the initial temperature. The following section explains the relationship between the heat flow and material properties of a contact object, which is the key physical phenomenon for thermal-based material identification.

B. HEAT FLOW AND MATERIAL PROPERTIES

When the gripper surface contacts the object, dissipating (outflow) and absorbing (inflow) heat flux (5) between the gripper surface (subscript g) and the objects (subscript o) are equal as

$$-\lambda_o \frac{\partial T_o}{\partial x_o} = \lambda_g \frac{\partial T_g}{\partial x_g} \tag{7}$$

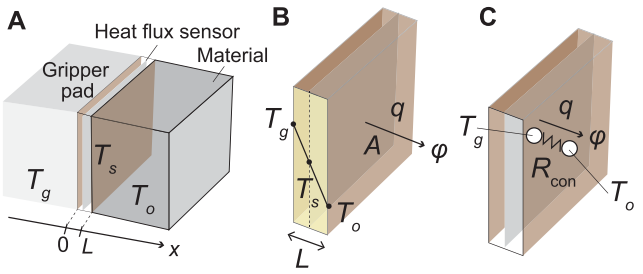

FIGURE 2. Thermal contact model. (*A*) T_g, T_o, and L denote the temperature [K] of the gripper, the temperature [K] of the object, and the heat transfer distance [m] (thickness of the heat flux sensor), respectively. (*B*) q, φ and A present heat flow [W], heat flux [W/m^2], and cross sectional area [m^2], respectively. (*C*) R_{con} is thermal contact resistance (*TCR*) [K/W].

In general, the thermal dynamics of two contacting materials can be expressed using the semi-infinite solid model [35], [41], [42], which is derived from (1) with the initial and boundary conditions ($T(x, 0) = T_i$ and $T(0, t) = T_s$) as

$$T(x, t) = T_s + (T_i - T_s)\,\mathrm{erf}\frac{x}{2\sqrt{\alpha t}}, \tag{8}$$

where erf is the Gauss error function, and the subscripts s and i present the contact surface and initial parameter, respectively. Using the model in (8), (7) can be rewritten as

$$-\left(T_{oi} - T_s\right)\frac{\lambda_o}{2\sqrt{\alpha_o t}} = \left(T_{gi} - T_s\right)\frac{\lambda_g}{2\sqrt{\alpha_g t}}, \tag{9}$$

where T_{oi} and T_{gi} denote the initial temperature of the object and the gripper, respectively. Therefore, the temperature of the contact surface between the gripper and the object is derived as

$$\begin{aligned} T_s &= \frac{T_{oi}\frac{\lambda_o}{\sqrt{\alpha_o}} + T_{gi}\frac{\lambda_g}{\sqrt{\alpha_g}}}{\frac{\lambda_o}{\sqrt{\alpha_o}} + \frac{\lambda_g}{\sqrt{\alpha_g}}} \\ &= \frac{T_{oi}\sqrt{\lambda_o \rho_o c_o} + T_{gi}\sqrt{\lambda_g \rho_g c_g}}{\sqrt{\lambda_o \rho_o c_o} + \sqrt{\lambda_g \rho_g c_g}} \end{aligned} \tag{10}$$

where ρ and c stand for the density and specific heat, respectively. Here, T_s is assumed to be in the steady state ($t = \infty$), which is converged to a constant value. The term $\sqrt{\lambda \rho c}$ presents a thermal effusivity (contact coefficient) [35], [41]; each material has its own parameters due to the thermal properties of the materials. Equation (10) means that the contact temperature depends on the material properties and the initial temperature of the gripper and the object. Therefore, thermal-based material identification has two drawbacks as follows:

1) The material properties cannot be revealed when the initial temperature of the gripper (T_g) and the object (T_o) are the same.
2) The temperature response for identification is affected by the initial temperature variations from environmental change, which causes accuracy degradation.

The active heat flow sensing proposed in this paper can solve these two issues; this is explained in the next section.

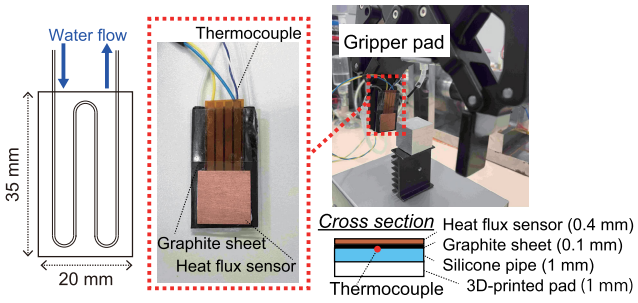

FIGURE 3. Design of the gripper pad for actively sensing temperature and heat flow. The silicone pipe was embedded in the thin bottom layer, and temperature-controlled water was circulated inside the pipe to regulate the surface temperature. The heat flow sensor is attached to the surface, monitoring thermal exchange through contacting an object.

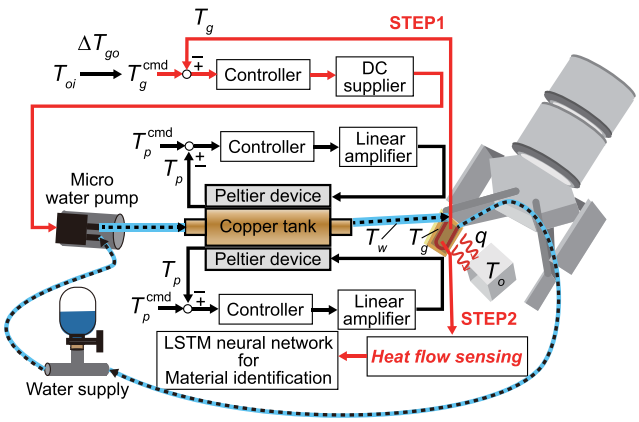

FIGURE 4. Overview of active heat flow sensing. **STEP 1:** Temperature control of the initial temperature of the gripper pad. **STEP 2:** Material identification by contacting (grasping) the object.

IV. PROPOSED ACTIVE HEAT FLOW SENSING

Our solutions to the above issues are as follows:

1) The temperature of the gripper surface is actively controlled to generate a temperature difference with the contact object, inducing heat flow for any kind of object.
2) The heat flow data, directly expresses the amount of thermal exchange, is used for material identification instead of temperature data to handle initial temperature variations.

In this paper, active temperature control is conducted using heat convection of a circulating water system, which consists of a micropump and a tank equipped with Peltier elements on both sides. The water system can switch between forced and natural convection at the gripper surface by controlling the water pump, regulating the gripper's initial temperature, and monitoring natural heat flow during contact. Thus, to monitor natural thermal exchange, it is more appropriate to mount the water circulation system on the contact surface rather than directly attaching the heat source (a similar mechanism to human thermal perception based on blood circulation). The water temperature is regulated by the Peltier devices, and the

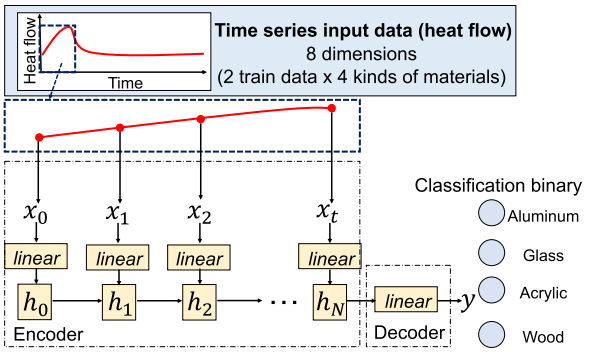

FIGURE 5. The learning process of the proposed method (Encoder-Decoder model). The input data of the learning system is the time-series heat flow responses of the gripper pad. The data was saved while the gripper contacted the object, and the 1-second data after contact, including a peak, was used for the LSTM neural network (two out of three trials were used for training and one for testing). The time-series heat flow input data are first processed by an encoder, which includes a linear layer ($N = 64$ nodes) and LSTM ($N = 64$ nodes) (see Appendix B). The encoded features are then processed by a decoder that outputs four (Scenario 1) or three (Scenario 2) material labels.

heat convection of the water flow between the Peltier device and the gripper is expressed as

$$C_w \frac{dT_w}{dt} = \frac{T_p - T_w}{R_w} - \frac{T_w - T_g}{R_g} \tag{11}$$

$$C_g \frac{dT_g}{dt} = \frac{T_w - T_g}{R_g} - \frac{T_g - T_a}{R_a}, \tag{12}$$

where T, C, and R denote the temperature, thermal capacitance, and thermal resistance of the Peltier device (p), water (w), gripper (g), and air (a), respectively. The temperature command of the gripper T_g^{cmd} is determined based on the initial temperature of the contact object (T_{oi}) as

$$T_g^{cmd} = T_{oi} \pm \Delta T_{go}, \tag{13}$$

where ΔT_{go} is the temperature difference between the gripper and the object, which can be set to the intended value. Thus, the contact temperature in (10) can be expressed as

$$T_s = T_{oi} \pm \frac{\Delta T_{go}}{1 + \frac{\sqrt{\lambda_o \rho_o c_o}}{\sqrt{\lambda_g \rho_g c_g}}}, \tag{14}$$

when the initial gripper temperature T_{gi} is controlled to the command T_g^{cmd} in (13). Equation (14) shows that the thermal exchange at the contact surface depends on ΔT_{go}, and T_s is constant when $T_{oi} = T_{gi}$ such that the second term in (14) becomes 0.

Fig. 3 shows the developed gripper pad for active heat flow sensing. The silicone pipe (outer diameter:1 mm) was embedded in the thin bottom layer, and temperature-controlled water was circulated inside the pipe. The surface temperature is uniformed by covering a graphite sheet, which has high heat conductivity. The CAPTEC's heat flux sensor was attached to the gripper surface, and a thermocouple (temperature sensor) was attached to the silicone pipe for comparison with heat flow sensing. The pad was attached to the robot

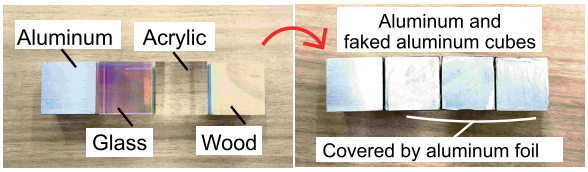

FIGURE 6. Target objects for material identification (aluminum, glass, acrylic, and wooden cubes). The three kinds of cubes (glass, acrylic, and wooden) were wrapped in aluminum foil to make it difficult to distinguish visual and tactile sensing. These materials were selected based on various thermal properties and high stiffness (hardness) so that the contact surface remains constant and the thermal-based method is valid.

TABLE 1. Scenario 1: Assessment of proposed active heat flow sensing (Case I-pro) compared with conventional passive sensing (Case I-cnv). The room temperature was 24 °C.

Case	Gripper	Contact object	Difference
Case I-cnv	34 °C	34 °C	0 °C
Case I-pro	44 °C	34 °C	10 °C

TABLE 2. Scenario 2: Assessment of robust material identification at various initial temperatures. The room temperature was 24 °C.

Case	Gripper	Contact object	Difference
Case I(-pro)	44 °C	34 °C	10 °C
Case II	34 °C	24 °C	10 °C
Case III	29 °C	19 °C	10 °C
Case IV	24 °C	34 °C	10 °C
Case V	19 °C	29 °C	10 °C

gripper (ROBOTIQ 2F-85), and it is in contact with the target object surface to monitor heat flow. Note that the heat flux sensor outputs were converted to heat flow by multiplying the sensor's surface area ($1.5\times10^{-2}\times1.5\times10^{-2}$ [m^2]).

The proposed active heat flow sensing overview is shown in Fig. 4. The strategy is divided into two steps: temperature control of the initial temperature of the gripper pad (STEP 1) and material identification by contacting (grasping) the object (STEP 2). In STEP 1, the initial temperature of the gripper is regulated by switching the micro water pump on and off based on the gripper temperature. The temperature of the Peltier devices is regulated by a *PI* controller referring to its command (T_p^{cmd}) in advance to heat/cool the water. Then, in STEP 2, after regulating the gripper's initial temperature, the gripper contacts the object and monitors the heat flow q, identifying materials using the LSTM neural network. The point is the gripper pad temperature can be regulated depending on the object temperature, being able to distinguish the materials in the various initial temperatures. The experimental results presented in the following sections use the obtained q (active heat flow sensing) and T_g (the gripper temperature for comparison) for material identification, suggesting the advantage of the proposed strategy.

The overview of the learning process (Encoder-Decoder model) in our system is shown in Fig. 5. The input data of the learning system is the time-series heat flow responses of

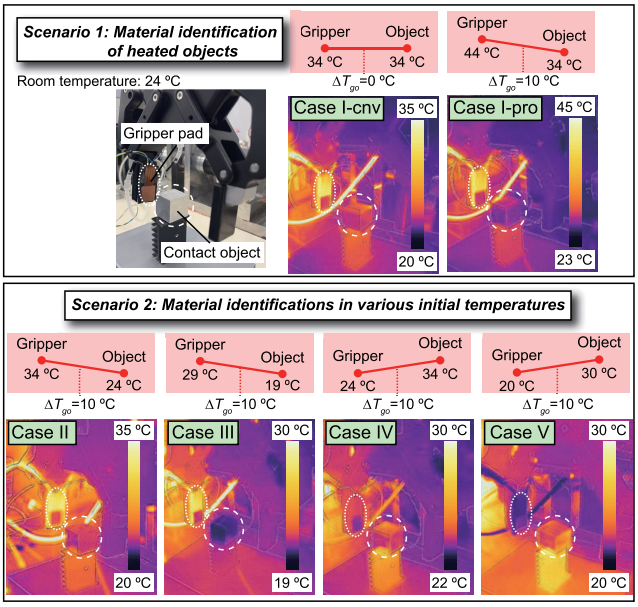

FIGURE 7. Several cases of experiments with various temperature differences between the gripper and the objects. Temperature settings in each scenario are summarized in Tables 1 (Scenario 1) and 2 (Scenario 2).

the gripper pad. We conducted experiments and saved the data thrice per material under the same condition, using two data for training and one for testing. The data was saved while the gripper contacted the object, and the 1-second data after contact, including a peak, was used for training the LSTM neural network (8 dimensions: two train data × four kinds of materials). The sampling time is 1 msec. As for the temperature data for comparison experiments, 5-second data were used for classification. The time-series heat flow input data are first processed by an encoder, which includes a linear layer (64 nodes) and LSTM (64 nodes) (see Appendix B). The encoded features are then processed by a decoder that outputs four (Scenario 1) or three (Scenario 2) material labels (see the following section).

V. EXPERIMENTAL VERIFICATION

A. EXPERIMENTAL OUTLINE

Fig. 6 shows four kinds of materials used as target objects: aluminum cubes, glass, acrylic, and wooden cubes wrapped in aluminum foil (2 cm×2 cm×2 cm). These three kinds of cubes (glass, acrylic, and wooden) were wrapped in aluminum foil to make it difficult to distinguish visual and tactile sensing. The materials were selected based on various thermal properties and high stiffness (hardness) so that the contact surface remains constant and the thermal-based method is valid.

In each experiment, the robot gripper was in contact with the object for 20 sec at 8.82 N, and the temperature and heat flow were monitored. We conducted experiments and saved the data thrice per material under the same condition, using two data for training the LSTM neural network and one for

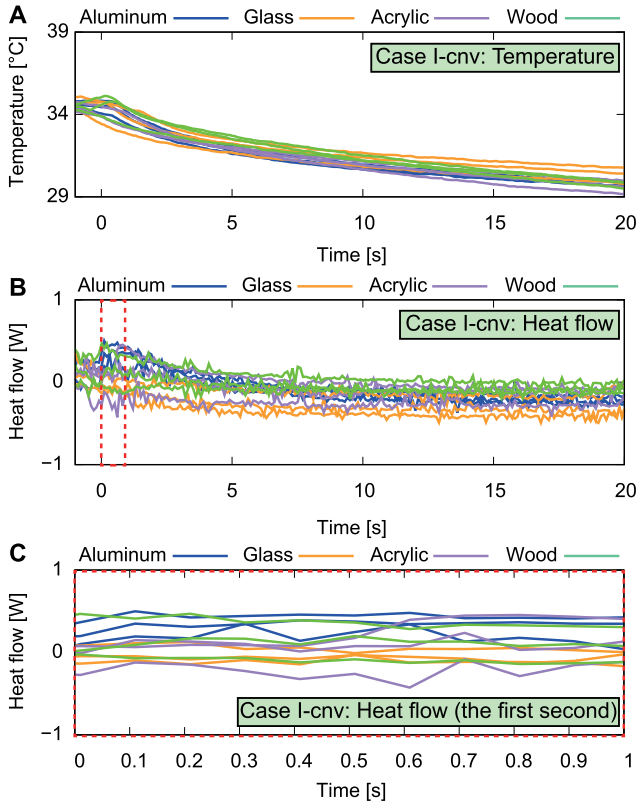

FIGURE 8. [Case I-cnv.] Thermal responses of the heated gripper (34 °C) in contact with the heated objects (34 °C): (*A*) Temperature; (*B*) Heat flow and (*C*) First 1 sec of the heat flow in (*B*). Two of three trials in each material were used for training and one for testing. These graphs are plotted by thinning out the sampling data to 1/10.

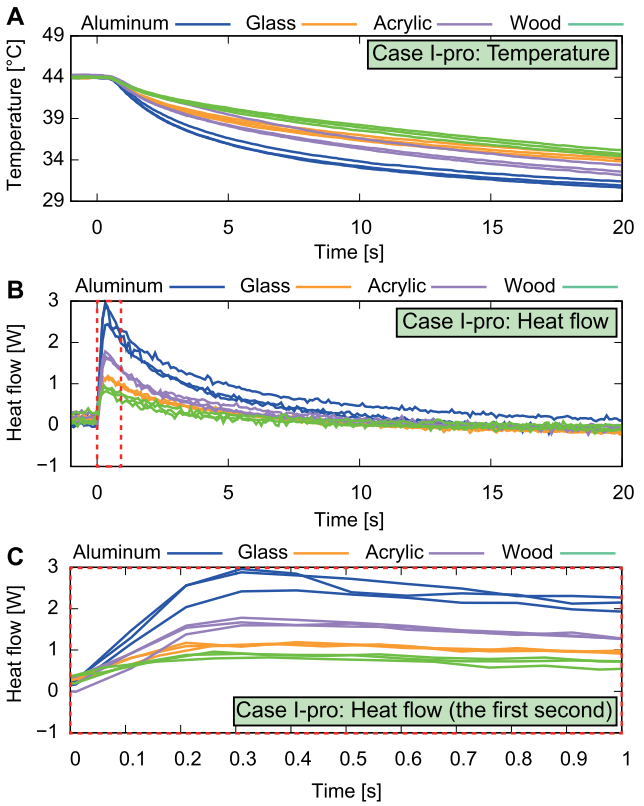

FIGURE 9. [Case I-pro.] Thermal responses of the heated gripper (44 °C) in contact with the heated objects (34 °C): (*A*) Temperature; (*B*) Heat flow and (*C*) First 1 sec of the heat flow in (*B*). Two of three trials in each material were used for training and one for testing. These graphs are plotted by thinning out the sampling data to 1/10.

testing. The temperature and heat flow responses for material identification were obtained in two scenarios (five cases) as follows (also see Fig. 7). Note that the room temperature was 24 °C in every case.

In Scenario 1, material identification of heated objects was conducted to assess the active heat flow sensing. Generally, thermal-based methods use passive control of a heater (ON/OFF switching), and most studies do not consider heated object recognition. Thus, the heated object's material identifications (ΔT_{go} =0), which cannot be identified using a conventional heater system, were conducted to show the advantage of active heat flow sensing. The contact object was heated to 34 °C in advance, and the classification results were compared with the active-controlled gripper (44 °C) and passive one (34 °C: conventional studies generally set the gripper temperature to around +10 °C from room temperature), see Table 1. The paper refers to the former case as [Case I-pro] (the proposed active control method) and the latter case as [Case I-cnv] (the conventional heating method), respectively.

In Scenario 2, material identifications in various initial temperatures were conducted using the active heat flow sensing system. As initial temperature variations are one of the drawbacks of conventional studies, the experiments were conducted to show the robustness of material identification against environmental change. Table 2 summarizes the temperature setting in each case.

B. EXPERIMENTAL RESULTS AND DISCUSSIONS

The temperature and heat flow responses in Case I-cnv and Case I-pro are shown in Figs. 8 and 9 (The plots in other cases are shown in Appendix C). Here, two of three trials in each material were used for training and one for testing. Using the obtained time series data, the success rate of classification in each case was compared in two ways and summarized in Figs 10 and 11. Here, the classification results are summarized using 0.1 to 1-second heat-flow data (0.1 sec interval) and temperature data of 1 sec to V sec (1.0 s interval) after contact, respectively. Each result (blue dot) is linearly interpolated with colored surfaces (blue to red gradient color shows low to high classification accuracies).

First, the classification accuracies of heated materials using the time series temperature and heat flow data in Case I-cnv and Case I-pro were compared to show the advantage of active heat flow sensing. Figs. 10A and B show the classification results of passive temperature and heat flow sensing, in which the gripper's temperature was set to +10 °C from room temperature (Case I-cnv). Since the temperature

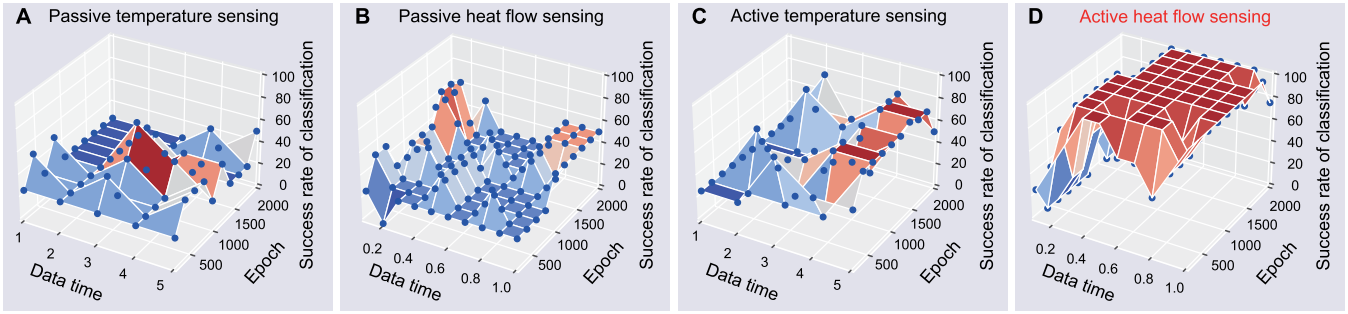

FIGURE 10. Classification accuracy (aluminum, glass, acrylic, wood) of heated materials (Scenario 1). The proposed active heat flow sensing (*D*) compared with active temperature sensing (*C*), passive heat flow (*B*) and temperature (*A*) sensing in [Case I]. The classification results are summarized using 0.1 to 1-second heat-flow data (0.1 sec interval) and temperature data of 1 sec to 5 sec (1.0 s interval) after contact, respectively. Each result (blue dot) is linearly interpolated with colored surfaces (blue to red gradient color shows low to high classification accuracies). The required data time based on heat flow sensing for reliable accuracy is less than that of temperature sensing. The active heat flow sensing is realized within 0.4 sec of first contact for 100 % classification accuracy (see *D*). In contrast, temperature sensing required 4 sec and 75 % classification due to the similarities in thermal properties between glass and acrylic (see *C*). Less heat exchange quantity causes a decrease in the classification success rate (see *A*, *B*).

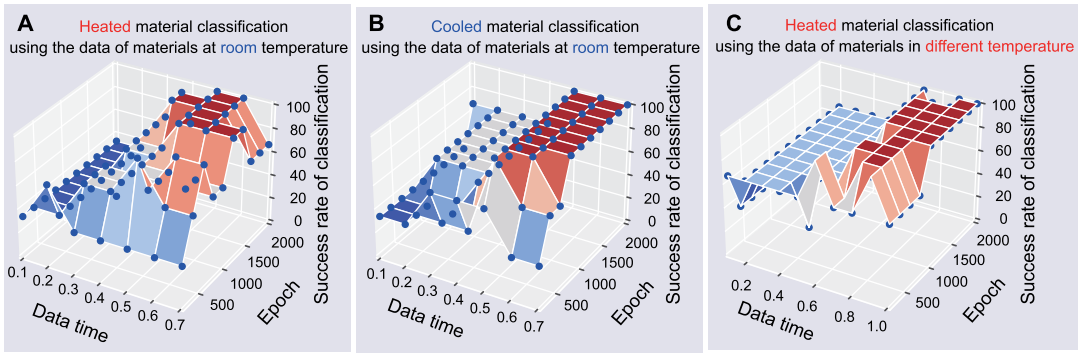

FIGURE 11. Classification accuracy (aluminum, glass, wood) of active heat flow sensing under different experimental conditions (Scenario 2). (*A*) Trained with the dataset [Case I-pro] and tested with [Case II]; (*B*) Trained with the dataset [Case I-pro] and tested with [Case III]; (*C*) Trained with the dataset [Case IV] and tested with [Case V]. In all cases, the materials were perfectly classified within 0.5 sec (see *A*, *B*) and 0.7 sec (see *C*). These results suggest robustness against environmental change between the training and test phases of the proposed active heat flow sensing strategy, which has been difficult using conventional temperature-based methods.

difference between the gripper and the object is almost 0 °C, the heat exchange quantity is less than that in other cases, and it is difficult to monitor the material properties from the temperature and heat flow responses (see Figs. 8). This causes a decrease in the classification success rate.

Figs. 10 C and D show the case of active temperature and heat flow sensing in which the gripper was actively controlled to + 20 °C from room temperature so that the temperature difference with the object remained at 10 °C. Thanks to the temperature difference, the material difference is revealed in the temperature and heat flow responses in Fig. 9.

In particular, the required data time based on heat flow sensing for reliable accuracy is less than that of temperature sensing. The active heat flow sensing is realized within 0.4 sec of first contact for 100 % classification accuracy. In contrast, temperature sensing required 4 sec, and 75 % classification due to the similarities in thermal properties between glass and acrylic.

Table 3 summarizes the classification results at 2000 epochs using the LSTM neural network compared with RNN, the straightforward and primary conventional method. The results show the proposed active heat flow sensing method achieves the highest classification accuracy. As the results can be derived using such simple strategies, it suggests that the proposed method works regardless of classification methods. The primary contribution of the paper is a novel system design to derive thermal data correction and identify the material. We used RNN-based methods as a time-serial identification model; however, we believe other identification models can be used instead.

According to the model in equation (10), thermal properties (thermal effusivity) appear in the steady state of the temperature response. Thus, temperature-based material classification takes time. On the other hand, heat flow (flow variable) depends on the temperature differential (effort variable), making it possible to obtain high classification accuracy in less time. Note that the time response limit of heat flow sensing in our system is 0.2 sec, and the recognition time can be faster by improving the hardware system.

Second, several classifications were conducted using the training and test data in different cases to emulate the environmental change (e.g., the temperature of the objects or the gripper changes from the training phase to the test phase). Here, the classification using the data under different conditions is more sensitive to the difference in the contact conditions and noise than the classification based on the data

TABLE 3. The accuracy of the material classification using RNN and LSTM neural network. The results show the proposed active heat flow sensing method achieves the highest accuracy regardless of classification methods.

	Time	RNN	LSTM
Active heat flow sensing (Case I-pro)	**0.4** s **1.0** s	**100** % **100** %	**100** % **100** %
Active temperature sensing (Case I-pro)	5 s	50 %	75 %
Passive heat flow sensing (Case I-cnv)	0.4 s 1.0 s	25 % 25 %	25 % 25 %
Passive temperature sensing (Case I-cnv)	5 s	25 %	25 %

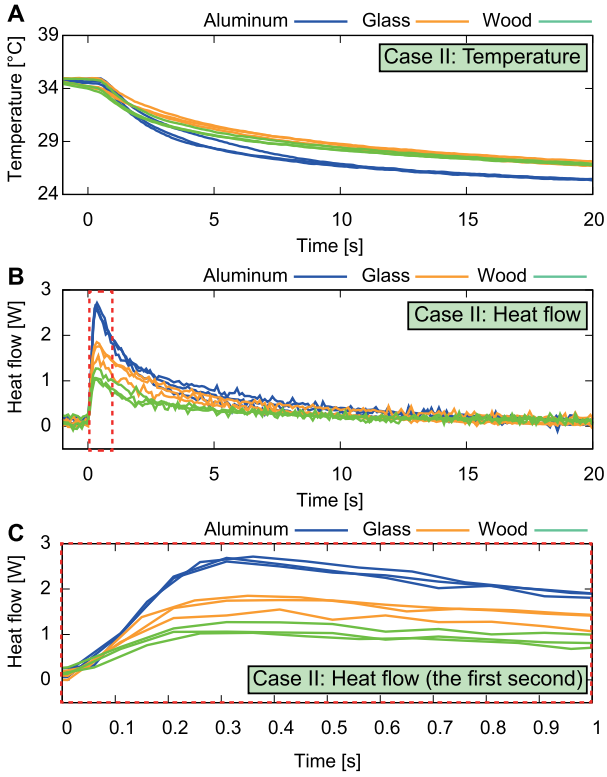

FIGURE 12. [Case II] Thermal responses of the heated gripper (34 °C) in contact with the objects (24 °C): (*A*) Temperature; (*B*) Heat flow and (*C*) First 1 sec of the heat flow in (*B*).

in the same situation. Thus, three materials (aluminum, glass, and wood) whose thermal properties are largely different are used as contact objects to show the possibility of perfect classification using heat flow in other conditions. The success rates are summarized in Fig. 11. In all cases, the materials were perfectly classified within 0.5 sec (Fig. 11A, B) and 0.7 sec (Fig. 11C). These results suggest robustness against environmental change between the training and test phases of the proposed active heat flow sensing strategy, which has been difficult using conventional temperature-based methods.

VI. SUMMARY

The paper presented the strategy for robust material identification based on heat flow sensing. The proposed system

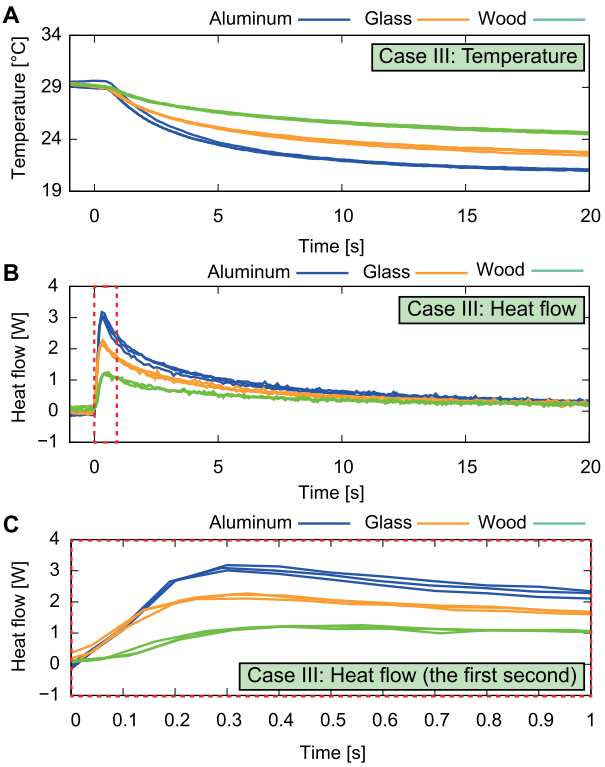

FIGURE 13. [Case III] Thermal responses of the heated gripper (29 °C) in contact with the cooled objects (19 °C): (*A*) Temperature; (*B*) Heat flow and (*C*) First 1 sec of the heat flow in (*B*).

can induce and monitor heat flow between a gripper and various material objects by actively controlling the robot gripper's surface temperature and extracting the objects' material properties for identification. The experimental results indicate the following advantages of active heat flow sensing:

- Rapid and high material classification can be realized. The response time of active heat flow sensing is faster and more precise than temperature sensing to reveal the material properties.
- Robust classification against the temperature variations of the object is realized by adjusting the initial temperature difference between the gripper and the objects.

These findings could be useful for developing multimodal sensing for dexterous robot manipulation to realize high-precision tasks such as detecting fine scratches or medical activities.

VII. FUTURE WORK

There are still some challenges to address, as outlined below. First, in this study, solid cubes with the same volume as the target object were used to fix the contact area. However, soft materials can be deformed by applying a grasping force, and heat flow sensing under changes in the thermal exchange area is needed. Second, thermal sensing is still sensitive to environmental change, and materials with similar thermal properties (e.g., acrylic and glass in this paper) are challenging to classify completely under different

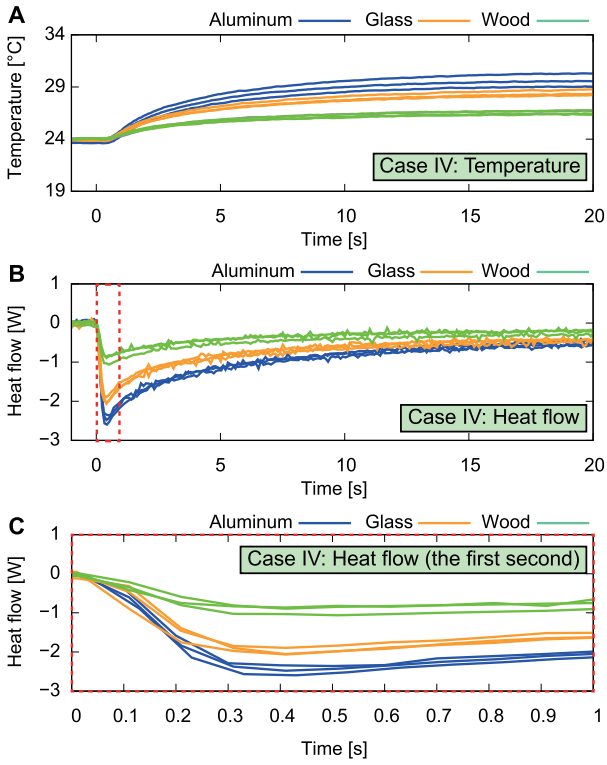

FIGURE 14. [Case IV] Thermal responses of the gripper (24 °C) in contact with the heated objects (34 °C): (*A*) Temperature; (*B*) Heat flow and (*C*) First 1 sec of the heat flow in (*B*).

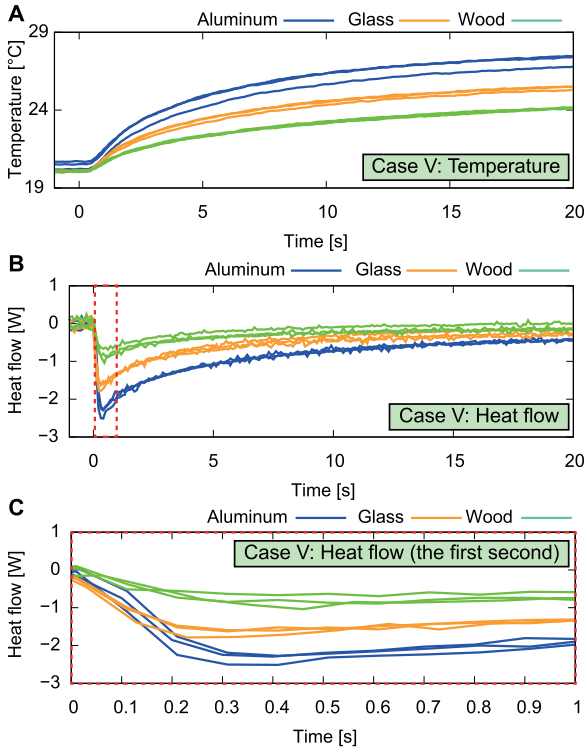

FIGURE 15. [Case V] Thermal responses of the cooled gripper (19 °C) in contact with the heated objects (29 °C): (*A*) Temperature; (*B*) Heat flow and (*C*) First 1 sec of the heat flow in (*B*).

initial temperatures. Integrating with other kinds of sensors (e.g., tactile, vision, etc.) might improve the classification accuracy; we plan to attempt this approach in the next phase. We will tackle these problems in our future work to realize a feasible recognition method based on thermal technology.

APPENDIX A
PSEUDO CODE OF THE NETWORK

The pseudo-code of the LSTM neural network is described in Algorithm 1. As for the overview of the learning process in our system, please see Fig. 5.

Algorithm 1 Thermal-based material classification using LSTM neural network

Require: x_t {heat flow dataset}
Require: y {material label dataset}
Require: Model {Learning Model that consists of encoder, LSTM layer, and decoder}
  for iteration i = 1, 2, ..., 5000 **do**
    for tep t = 0,1,...,N-1 **do**
      if t = 0 **then**
        $h_t = 0$
      end if
      h'_t = encoder(x_t)
      $h_{t+1} \leftarrow$ LSTM(h'_t, h_t)
    end for
    $\hat{y} \leftarrow$ decoder(h_{t+1})
    Loss $\leftarrow$ cross_entropy($\hat{y}$, y) {update Model parameters by BPTT}
  end for

APPENDIX B
PARAMETER OPTIMIZATION OF THE NETWORK

We confirmed the parameter setting of the LSTM neural network by trying several combinations of the number of nodes of the linear layer and LSTM using the data in Fig. 9 as shown in Table 4. From Table 4, all combinations, except the case that the nodes of the linear layer and LSTM are set to 16, can obtain 100 % classification results. We chose the number of nodes as 64 and conducted classifications.

TABLE 4. Several combinations of the number of nodes of the linear layer and LSTM.

Linear Layer	LSTM Layer	Classification accuracy
16	16	75%
32	32	100%
64	64	100%
128	128	100%

APPENDIX C
THERMAL RESPONSES (RAW DATA) IN CASES II–V

The temperature and the heat flow responses in Case II, III, IV, V are shown in Figs. 12–15. Two of three trials in each material were used for training and one for testing.

ACKNOWLEDGMENT

The authors thank Ixchel Ramirez, one of their colleagues, for reviewing and giving them valuable advice.

REFERENCES

[1] W. M. B. Tiest, "Tactual perception of material properties," *Vis. Res.*, vol. 50, no. 24, pp. 2775–2782, Dec. 2010.

[2] B. Ma, Z. Liu, F. Jiang, Y. Yan, J. Yuan, and S. Bu, "Vehicle detection in aerial images using rotation-invariant cascaded forest," *IEEE Access*, vol. 7, pp. 59613–59623, 2019.

[3] G. Schwartz and K. Nishino, "Recognizing material properties from images," *IEEE Trans. Pattern Anal. Mach. Intell.*, vol. 42, no. 8, pp. 1981–1995, Aug. 2020.

[4] H. Alagi, A. Heiligl, S. E. Navarro, T. Kroegerl, and B. Hein, "Material recognition using a capacitive proximity sensor with flexible spatial resolution," in *Proc. IEEE/RSJ Int. Conf. Intell. Robots Syst. (IROS)*, Oct. 2018, pp. 6284–6290.

[5] Y. Ding, H. Kisner, T. Kong, and U. Thomas, "Using machine learning for material detection with capacitive proximity sensors," in *Proc. IEEE/RSJ Int. Conf. Intell. Robots Syst. (IROS)*, Oct. 2020, pp. 10424–10429.

[6] S. E. Navarro, S. Mühlbacher-Karrer, H. Alagi, H. Zangl, K. Koyama, B. Hein, C. Duriez, and J. R. Smith, "Proximity perception in human-centered robotics: A survey on sensing systems and applications," *IEEE Trans. Robot.*, vol. 38, no. 3, pp. 1599–1620, Jun. 2022.

[7] R. N. Khushaba and A. J. Hill, "Radar-based materials classification using deep wavelet scattering transform: A comparison of centimeter vs. Millimeter wave units," *IEEE Robot. Autom. Lett.*, vol. 7, no. 2, pp. 2016–2022, Apr. 2022.

[8] C. Fang, D. Wang, D. Song, and J. Zou, "Fingertip pulse-echo ultrasound and optoacoustic dual-modal and dual sensing mechanisms near-distance sensor for ranging and material sensing in robotic grasping," in *Proc. IEEE Int. Conf. Robot. Autom. (ICRA)*, May 2021, pp. 14105–14111.

[9] T. Kubiczek and J. C. Balzer, "Material classification for terahertz images based on neural networks," *IEEE Access*, vol. 10, pp. 88667–88677, 2022.

[10] S. Luo, J. Bimbo, R. Dahiya, and H. Liu, "Robotic tactile perception of object properties: A review," *Mechatronics*, vol. 48, pp. 54–67, Dec. 2017.

[11] A. Yamaguchi and C. G. Atkeson, "Recent progress in tactile sensing and sensors for robotic manipulation: Can we turn tactile sensing into vision?" *Adv. Robot.*, vol. 33, no. 14, pp. 661–673, Jul. 2019.

[12] S. S. Baishya and B. Bäuml, "Robust material classification with a tactile skin using deep learning," in *Proc. IEEE/RSJ Int. Conf. Intell. Robots Syst. (IROS)*, Oct. 2016, pp. 8–15.

[13] A. Schmitz, Y. Bansho, K. Noda, H. Iwata, T. Ogata, and S. Sugano, "Tactile object recognition using deep learning and dropout," in *Proc. IEEE-RAS Int. Conf. Humanoid Robots*, Nov. 2014, pp. 1044–1050.

[14] W. Yuan, C. Zhu, A. Owens, M. A. Srinivasan, and E. H. Adelson, "Shape-independent hardness estimation using deep learning and a GelSight tactile sensor," in *Proc. IEEE Int. Conf. Robot. Autom. (ICRA)*, May 2017, pp. 951–958.

[15] M. Neumann, K. Nottensteiner, I. Kossyk, and Z.-C. Marton, "Material classification through knocking and grasping by learning of structure-borne sound under changing acoustic conditions," in *Proc. IEEE 14th Int. Conf. Autom. Sci. Eng. (CASE)*, Aug. 2018, pp. 1269–1275.

[16] W. Yuan, Y. Mo, S. Wang, and E. H. Adelson, "Active clothing material perception using tactile sensing and deep learning," in *Proc. IEEE Int. Conf. Robot. Autom. (ICRA)*, May 2018, pp. 4842–4849.

[17] W. Yuan, S. Wang, S. Dong, and E. Adelson, "Connecting look and feel: Associating the visual and tactile properties of physical materials," in *Proc. IEEE Conf. Comput. Vis. Pattern Recognit. (CVPR)*, Jul. 2017, pp. 4494–4502.

[18] K. Takahashi and J. Tan, "Deep visuo-tactile learning: Estimation of tactile properties from images," in *Proc. Int. Conf. Robot. Autom. (ICRA)*, May 2019, pp. 8951–8957.

[19] C. H. Lin, T. W. Erickson, J. A. Fishel, N. Wettels, and G. E. Loeb, "Signal processing and fabrication of a biomimetic tactile sensor array with thermal, force and microvibration modalities," in *Proc. IEEE Int. Conf. Robot. Biomimetics (ROBIO)*, Dec. 2009, pp. 129–134.

[20] Y. Gao, L. A. Hendricks, K. J. Kuchenbecker, and T. Darrell, "Deep learning for tactile understanding from visual and haptic data," in *Proc. IEEE Int. Conf. Robot. Autom. (ICRA)*, May 2016, pp. 536–543.

[21] T. Bhattacharjee, H. M. Clever, J. Wade, and C. C. Kemp, "Multimodal tactile perception of objects in a real home," *IEEE Robot. Autom. Lett.*, vol. 3, no. 3, pp. 2523–2530, Jul. 2018.

[22] G. Cheng, E. Dean-Leon, F. Bergner, J. R. G. Olvera, Q. Leboutet, and P. Mittendorfer, "A comprehensive realization of robot skin: Sensors, sensing, control, and applications," *Proc. IEEE*, vol. 107, no. 10, pp. 2034–2051, Oct. 2019.

[23] Z. Erickson, E. Xing, B. Srirangam, S. Chernova, and C. C. Kemp, "Multimodal material classification for robots using spectroscopy and high resolution texture imaging," in *Proc. IEEE/RSJ Int. Conf. Intell. Robots Syst. (IROS)*, Oct. 2020, pp. 10452–10459.

[24] W. Yang, M. Xie, X. Zhang, X. Sun, C. Zhou, Y. Chang, H. Zhang, and X. Duan, "Multifunctional soft robotic finger based on a nanoscale flexible temperature–pressure tactile sensor for material recognition," *ACS Appl. Mater. Interface*, vol. 13, no. 46, pp. 55756–55765, Nov. 2021.

[25] D. Siegel, I. Garabieta, and J. Hollerbach, "An integrated tactile and thermal sensor," in *Proc. IEEE Int. Conf. Robot. Autom.*, Apr. 1986, pp. 1286–1291.

[26] R. A. Russell, "Thermal sensor for object shape and material constitution," *Robotica*, vol. 6, no. 1, pp. 31–34, Jan. 1988.

[27] G. J. Monkman and P. M. Taylor, "Thermal tactile sensing," *IEEE Trans. Robot. Autom.*, vol. 9, no. 3, pp. 313–318, Jun. 1993.

[28] M. Benali-Khoudjal, M. Hafez, J.-M. Alexandre, J. Benachour, and A. Kheddar, "Thermal feedback model for virtual reality," in *Proc. MHS Int. Symp. Micromechatronics Hum. Sci.*, Oct. 2003, pp. 153–158.

[29] J. Engel, N. Chen, C. Tucker, C. Liu, S.-H. Kim, and D. Jones, "Flexible multimodal tactile sensing system for object identification," in *Proc. 5th IEEE Conf. Sensors*, Oct. 2006, pp. 563–566.

[30] S. Takamuku, T. Iwase, and K. Hosoda, "Robust material discrimination by a soft anthropomorphic finger with tactile and thermal sense," in *Proc. IEEE/RSJ Int. Conf. Intell. Robots Syst.*, Sep. 2008, pp. 3977–3982.

[31] D. Xu, G. E. Loeb, and J. A. Fishel, "Tactile identification of objects using Bayesian exploration," in *Proc. IEEE Int. Conf. Robot. Autom.*, May 2013, pp. 3056–3061.

[32] A. Yamamoto, B. Cros, H. Hashimoto, and T. Higuchi, "Control of thermal tactile display based on prediction of contact temperature," in *Proc. IEEE Int. Conf. Robot. Autom. (ICRA)*, Apr. 2004, pp. 1536–1541.

[33] M. Guiatni, A. Benallegue, and A. Kheddar, "Thermal display for telepresence based on neural identification and heat flux control," *Presence*, vol. 18, no. 2, pp. 156–169, Apr. 2009.

[34] H.-N. Ho and L. A. Jones, "Contribution of thermal cues to material discrimination and localization," *Perception Psychophys.*, vol. 68, no. 1, pp. 118–128, Jan. 2006.

[35] H.-N. Ho, "Material recognition based on thermal cues: Mechanisms and applications," *Temperature*, vol. 5, no. 1, pp. 36–55, Jan. 2018.

[36] E. Kerr, T. M. McGinnity, and S. Coleman, "Material classification based on thermal properties—A robot and human evaluation," in *Proc. IEEE Int. Conf. Robot. Biomimetics (ROBIO)*, Dec. 2013, pp. 1048–1053.

[37] V. Chu, I. Mcmahon, L. Riano, C. G. McDonald, Q. He, J. Martinez Perez-Tejada, M. Arrigo, T. Darrell, and K. J. Kuchenbecker, "Robotic learning of haptic adjectives through physical interaction," *Robot. Auto. Syst.*, vol. 63, pp. 279–292, Jan. 2015.

[38] K. Katoh, Y. Ichikawa, E. Iwase, K. Matsumoto, and I. Shimoyama, "Material discrimination by heat flow sensing," in *Proc. TRANSDUCERS Int. Solid-State Sensors, Actuat. Microsyst. Conf.*, Jun. 2009, pp. 1549–1552.

[39] T. Bhattacharjee, J. Wade, and C. C. Kemp, "Material recognition from heat transfer given varying initial conditions and short-duration contact," *Robot., Sci. Syst.*, Jul. 2015, doi: 10.15607/RSS.2015.XI.019.

[40] T. Bhattacharjee, H. M. Clever, J. Wade, and C. C. Kemp, "Material recognition via heat transfer given ambiguous initial conditions," *IEEE Trans. Haptics*, vol. 14, no. 4, pp. 885–896, Oct. 2021.

[41] G.-H. Yang, D.-S. Kwon, and L. A. Jones, "Spatial acuity and summation on the hand: The role of thermal cues in material discrimination," *Perception Psychophys.*, vol. 71, no. 1, pp. 156–163, Jan. 2009.

[42] Y. Osawa, K. Kase, Y. Domae, Y. Furukawa, and A. Kheddar, "Material classification using active temperature controllable robotic gripper," in *Proc. IEEE/SICE Int. Symp. Syst. Integr. (SII)*, Jan. 2022, pp. 479–484.

YUKIKO OSAWA (Member, IEEE) received the B.E. degree in system design engineering and the M.E. and Ph.D. degrees in integrated design engineering from Keio University, Yokohama, Japan, in 2015, 2016, and 2019, respectively. She was a Research Fellow with the Japan Society for the Promotion of Science (JSPS), from 2017 to 2019. From 2019 to 2021, she was a JSPS Overseas Research Fellow and a Postdoctoral Researcher with CNRS, LIRMM, France, involved in Interactive Digital Humans (IDH) Team. She is currently with the National Institute of Advanced Industrial Science and Technology (AIST), Japan. Her research interests include human interface, human–robot interaction, haptics, and thermal systems. She is a member of SICE, RSJ, and IEEJ. She was a recipient of the Distinguished Paper Award from the Institute of Electric Engineers of Japan (IEEJ), in 2017; the Japan Society for the Promotion of Science (JSPS) Ikushi Award, in 2018; and the SICE International Young Authors Award, in 2022.

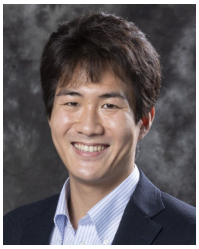

KEI KASE (Member, IEEE) received the B.E., M.E., and Ph.D. degrees from Waseda University, in 2017, 2019, and 2022, respectively. He was a Research Assistant with the National Institute of Advanced Industrial Science and Technology (AIST), Japan, from 2019 to 2023. He was a recipient of the IBM Ph.D. Fellowship, in 2019. His research interests include manipulation methods using deep learning, human–robot interactions, motor babbling, and symbol grounding.

YOSHIYUKI FURUKAWA received the B.E., M.E., and Ph.D. degrees in geometric modeling for computer-aided design from The University of Tokyo, in 1998, 2000, and 2003, respectively. He is a Research Team Leader with the Industrial Cyber-Physical Systems (ICPS) Research Center, National Institute of Advanced Industrial Science and Technology (AIST), Japan. He is leading the Connected Factory Research Team, to advance core technologies related to smart manufacturing and ICPS for manufacturing. In 2003, he joined AIST, where he has been developing technologies to support informatization and digitalization in manufacturing industry, especially small and medium-sized enterprises in Japan.

YUKIYASU DOMAE (Member, IEEE) received the B.E., M.E., and Ph.D. degrees from Hokkaido University, Japan, in 2004, 2006, and 2012, respectively. From 2008 to 2013, he was a Researcher with the Image Recognition Systems Group, Advanced Technology Research and Development Center, Mitsubishi Electric Corporation, Japan, where he was also a Principal Researcher, from 2013 to 2018. In 2018, he joined the National Institute of Advanced Industrial Science and Technology as the Group Leader of the Manipulation Research Group, where he has been a Team Leader of the Automation Research Team, since 2019. His research interests include machine vision and manipulation.